MedChemComm

Accepted Manuscript

ROYAL SOCIETY OF CHEMISTRY

www.rsc.org/medchemcomm

Journal Name

RSCPublishing

ARTICLE

Decorated 6,6',7,7'-tetrahydro-1*H*,1'*H*-2,3'-biindole scaffold as promising candidate for recognition of CDK2 allosteric site

Cite this: DOI: 10.1039/x0xx00000x

Received 00th January 2012,
Accepted 00th January 2012

DOI: 10.1039/x0xx00000x

www.rsc.org/

Antonio Rescifina,[a] Angela Scala,[*,b] Maria Teresa Sciortino,[*,c] Ivana Colao,[c] Gabriel Siracusano,[c] Antonino Mazzaglia,[d] Ugo Chiacchio,[a] and Giovanni Grassi[b]

The progression through S phase of cell cycle is controlled by cyclin-dependent kinase 2 (CDK2), the activity of which depends on its binding to regulatory partners (cyclins E and A). Deregulation of the activity of CDK2 has been associated with several sickness, such as infectious, neurodegenerative, and proliferative diseases. Based on these data, CDK2 has become an attractive target for the development of new anticancer drugs. Indoledione derivatives have recently received special attention in virtue of their pronounced biological effects, such as antiproliferative, antioxidant and antimicrobial properties. In the present work we have investigated the antiproliferative effect of an indolone-based derivative, namely DPIT, whose synthesis we have recently reported, with the aim to clarify its mechanism of action. Furthermore, docking studies have been performed on the eight stereoisomers of DPIT to investigate their capacity to interact as ligand with ortho- or allosteric sites of CDK2. The encouraging results showed DPIT as promising candidate to a new type 3 class of inhibitors of CDK2 that act recognizing the allosteric site.

1. Introduction

Appropriate regulation of the cell cycle is vital for development, cell growth and differentiation.[1] However alteration of the cell cycle is one of the main deregulations in the transformation of a normal cell to a cancerous cell and hence the genes and proteins regulating this process serve as key therapeutic targets.

The family of cyclin-dependent kinases (CDKs) is one of the main players that govern cell cycle progression. CDKs' activity is regulated at multiple levels: transcriptionally, post-translationally and by CDK inhibitors (CKIs). The CDK proteins are active only when forming a complex with their corresponding cyclin.

Among the CDK proteins, CDK2 is involved in the G1/S checkpoint and drives the cell cycle through the S phase. During G1/S transition, CDK2 complexed with cyclin E causes the phosphorylation of pRb proteins family,[2] hyperphosphorylated pRb dissociates from E2F family members, promoting the activation of E2F-dependent S phase specific gene expressions and consequently the entry in S phase. When the G1/S checkpoint is compromised, this leads to the initiation of the S or M phase despite cellular damage and results in cancerous cells.

Thus, CDK2 is a very attractive target for cancer therapy, as its overexpression is commonly observed in breast, ovarian and oral cancers, and correspondingly its inhibitors (CDKIs) can represent a novel class of chemotherapeutic agents.[3] Currently, available CDKIs primarily target the highly conserved ATP binding site and generally inhibit both cell cycle and transcriptional CDKs potentially leading to toxicities in normal cells.[4,5]

Thus, the search of novel alternative CDKIs with different mechanism of action is gaining increasing importance, in order to circumvent the problem of undesirable off target interactions.

In the framework of our studies dealing with the design of poly functionalized heterocycles,[6-13] we have recently reported a new class of aldol-type compounds[14] from water-soluble indole-3,4-diones[15] as novel anti-HSV-1 agents, sharing structural features with some CDKIs. In fact, many indoles or azaindoles containing derivatives showed an interesting inhibition of various kinases.[16]

These findings encouraged us to further expand our studies on the biological usefulness of our indolone derivatives, focusing on the most promising compound DPIT (Fig. 1), which has revealed the highest anti-HSV-1 activity *in vitro*, without cytotoxic effect on cells.[14]

Compounds currently used against HSV are able to interfere as a competitive inhibitor/alternate substrate with the viral DNA polymerase. The specific phosphorylation of such compounds is exerted by the HSV-induced viral TK (thymidine kinase) protein. Thus we carried out experiments on our indolones using HSV-1 TK minus viruses, finding that viral protein TK is not required for the antiviral activity in our experimental model (data not shown). The discovery that CDKIs inhibit HSV replication through novel mechanisms played a major role in the new appreciation of cellular proteins as potential targets for antivirals.

On this basis, we hypothesize that the indolone scaffold exerts an anti-proliferative effect on cellular growth, involving CDKs, which downstream could negatively regulate the viral replication.

In the present work, we wanted to analyze first the effect of DPIT on cell proliferation in normal and tumor cells. Therefore, we attempt to understand the mechanism of action of the drug and the drug-target binding by molecular docking studies using computational methods to examine protein-drug interactions of DPIT with CDK2. Finally we analyzed in *in vitro* cellular model the involvement on the key regulatory proteins such as CDK2/cyclin E.

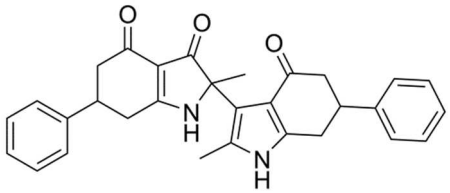

Fig. 1 Chemical structure of 2,2'-dimethyl-6,6'-diphenyl-6,6',7,7'-tetrahydro-1*H*,1'*H*-2,3'-biindole-3,4,4'(2*H*,5*H*,5'*H*)-trione (DPIT).

2.1. Treatment with DPIT affects cell viability

To assess the effect of DPIT on cell proliferation, the number of viable cells was evaluated by using the CellTiter-Glo® Luminescent Cell Viability Assay in normal and tumor cells. Three different cell types with different characteristics and origins were used. In particular Vero, HEp-2 and HEK 293 T cells were treated with DPIT at the final concentrations of 80, 90 and 100 μM for 24 h, 48 h and 72 h, and ATP levels, which indicate the presence of metabolically active cells, were measured. No significant reduction in terms of cell viability was detected in DPIT-treated Vero cells and HEK 293T cells at 24 h, whereas a more evident decrease was detected in HEp-2 treated cells compared to the controls at the same experimental time. At 48 h and 72 h the number of viable treated cells decreased in all cell lines compared to the untreated cells and, in particular, HEp-2 cells showed the hugest reduction. Furthermore, it has been observed that in addition to its time-dependent action, DPIT affects the viability of the three cell lines in a concentration-dependent manner (Fig. 2).

2. Results and discussion

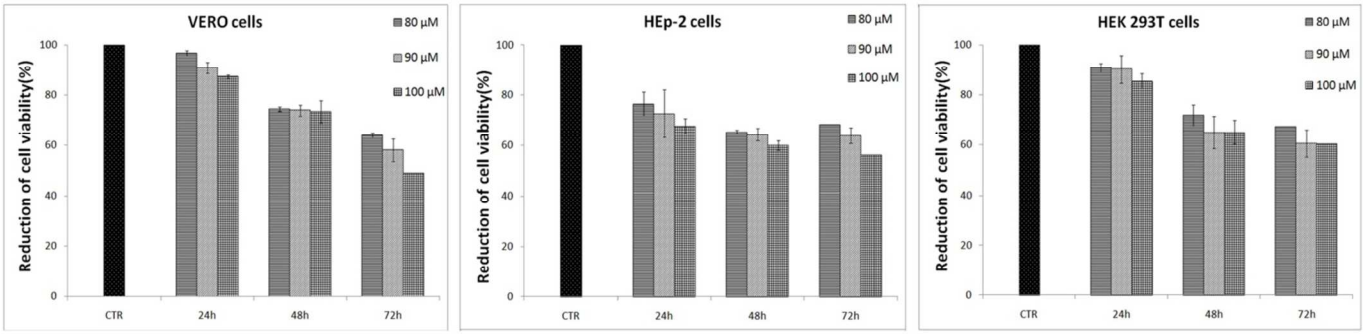

Fig. 2 The cell viability of VERO, HEp-2 and HEK 293 T cells was analyzed at 24, 48, 72 h of incubation in the presence of DPIT at concentration of 80, 90 and 100 μM. Untreated cells were used as control. CellTiter-Glo® Luminescent Cell Viability Assay Kit was used. The data are shown as means of triplicate. Error bars indicate the means ± SD of three independent experiments.

2.2. Molecular modeling

In order to rationalize the above biological results we have investigated, by *in silico* molecular modeling studies, the capacity of DPIT to act as an inhibitor of CDK2. Generally spoken, the Ser/Thr kinase inhibitors scenario, and then even the CDK2 one, although with slight differences, has been organized into five distinct groups:[17,18] type 1 constitutes the majority of ATP competitive inhibitors and recognizes the principal hydrophobic pocket in the so-called active conformation of the kinase (i.e. the kinase bonded with cycline, also referred as DFG-in); type 2 recognize the inactive conformation (DFG-out) that expose an additional hydrophobic binding site directly adjacent to the ATP binding one; type 3 that binds to an allosteric site near to the ATP binding one; type 4 that compete to protein kinase substrate (i.e. cyclins); and type 5 that covalently binds, in an irreversible manner, into the kinase active site by reacting with a nucleophilic cysteine residue.

Due to its chemical and structural characteristics, DPIT is unable to interact with the binding site of cyclins and to form covalent bonds in the primary active site, then only the first three types of interactions are possible.

So, we focalized our attention to the search, in the RCSB Protein Data Bank, for X-ray structures of CDK2 in complex with these typologies of ligand. After a careful evaluation the following structures have been identified as representative: 3F5X (CDK2/cyclin A, type 1),[19] 3EZV (type 2),[19] 3PXF (type 3),[20] and finally 3PY1 (types 2 and 3 concurrently)[20] for a competitive study.

As regards DPIT, all eight possible stereoisomers have been screened. To obtain the best and reliable docking results, for each complex, we first performed a molecular dynamics (MD) simulation of 1 ns in a physiological environment (pH 7.2, H_2O, NaCl 0.9%) to reduce the clashscore, i.e. the number of serious steric overlaps (> 0.4 Å) per 1000 atoms, and permit the ligand to best accommodate in the pocket, and successively each ligand were docked by Lamarckian genetic algorithm. The time of 1 ns was chosen, as the best cost/benefit ratio, after a preliminary screening on the 3EZV structure during 10 ns of MD simulation; the differences in binding energy obtained after10 ns were very negligible to justify this long run time. The docking results are reported in Table 1.

Table 1 Calculated Binding Energies (kcal/mol) to Catalytic Site of Types 1–3 for All Stereoisomers of DPIT and Co-crystallized Ligands.

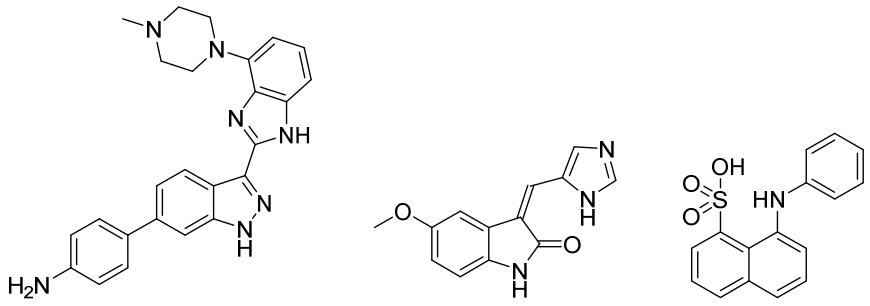

Entry	Ligand	Type 1 (3F5X)	Type 2 (3EZV)	Type 3 (3PXF)	Types 2 and 3 (3PY1)
1	(*R*,*R*,*R*)-DPIT	–11.31	–12.00	–12.42	–13.28
2	(*R*,*R*,*S*)-DPIT	–11.22	–12.75	–12.02	–12.97
3	(*R*,*S*,*R*)-DPIT	–11.70	–11.31	–11.96	–13.40
4	(*R*,*S*,*S*)-DPIT	–11.06	–11.42	–11.81	–13.24
5	(*S*,*R*,*R*)-DPIT	–10.89	–11.71	–12.40	–13.27
6	(*S*,*R*,*S*)-DPIT	–10.96	–11.91	–12.26	–13.34
7	(*S*,*S*,*R*)-DPIT	–11.79	–11.84	–12.40	–13.25
8	(*S*,*S*,*S*)-DPIT	–11.83	–11.68	–12.17	–12.77
9	EZV	–13.11	–12.83	—	—
10	SU9516	—	—	—	–9.45
11	ANS	—	—	–12.69	–13.95

It is evident that for representative type 1 group DPIT is much less active than EZV, whereas for type 2 group (*R*,*R*,*S*)-DPIT stereoisomer (entry 2) is active almost as much as the EZV (IC_{50} = 1 μM).[19] These data show that DPIT could act as a CDK2 ligand of types 1 and 2. Regarding to type 3 allosteric interactions DPIT is active almost as much as the ANS (IC_{50} = 91 μM, in this case the allosteric site is occupied by two ANS molecules). Finally, to understand if DPIT is better as type 2 or 3 ligand, we performed a competitive experiment using a X-ray CDK2 structure (3PY1) co-crystallized with both orthosteric and allosteric ligands (SU9516 and ANS, respectively) with a grid box sufficiently large to encompass both sites. In this case both SU9615 and ANS ligands, for all 100 docking pose, occupied the respective orthosteric and allosteric sites, whereas DPIT, for all 100 docking pose, occupied exclusively the allosteric site again with a binding energy very close to that of the ANS ligand. Combining the data, it can be deduced that DPIT could act as ligand to allosteric site of CDK2 with an IC_{50} slightly higher than 91 μM. This is in accord with the biological results, in fact the tight interaction of the CDK2/cyclin A complex (Kd = 48 nM)[21] requires that the allosteric inhibitor is very powerful. This picture can be also extended to CDK2/cyclin E complex; in fact, the CDK2/cyclin interface area is 3252 $Å^2$ in cyclin E[22] and 2839 $Å^2$ in cyclin A[23], then the former, having a larger area available for interactions between the two complexes, establish a bit stronger binding affinity for CDK2, as confirmed experimentally. So DPIT is readily displaced from CDK2 upon interactions with cyclins exhibiting a relatively weak inhibitory potency against the activated CDK2/cyclin complex and virtually no activity on HEp-2 and VERO cells. For that concern the stereochemistry almost all stereoisomers of DPIT are equipotent.

The best docked pose of (*R*,*R*,*R*)-DPIT with amino acidic interactions in the allosteric site of CDK2 (3PXF) is represented in Fig. 3 in both 2D and 3D arrangement (top and center). All interactions are hydrophobic, of van der Waals type, with 16 non polar amino acids (Leu 37, 55, 58, 66, 76, 78, 148; Val 44, 64, 154, 156; Ile 35, 52; Lys 56; Tyr 15, and Phe 80) and, unlike the two ANS molecules, one phenyl moiety of DPIT occupies a small hydrophobic pocket, located laterally with respect to the main cavity, constituted by three Val residues (44, 154, 156), two Leu residues (37, 76) and the Ile 35 one. This difference respect to ANS is clearly visible on the bottom of Fig. 3.

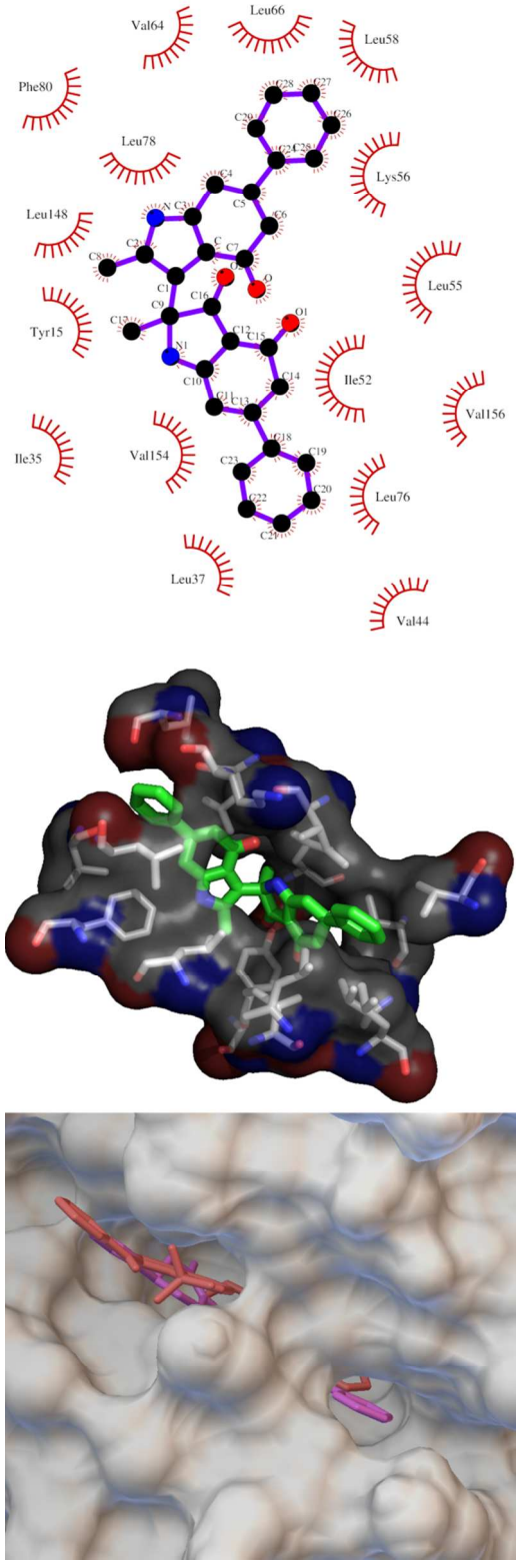

Fig. 3 (*R*,*R*,*R*)-DPIT complexed with 3PXF from docking. 2D Schematic view of hydrophobic interactions (top); 3D analogue, the ligand is represented as large tube whereas amino acids as small tube (center); superposition of the best docked pose for both (*R*,*R*,*R*)-DPIT (purple) and ANS (pink) (bottom). 2D plot was prepared with LigPlot+.[41]

2.3. CDK2/cyclin E complex is involved in the biological activity of DPIT

To plainly confirm the *in silico* molecular modeling data of DPIT in target the regulator proteins involved in cell cycle progression from G1 to S phases, a western blot analysis was performed to evaluate the accumulation of cyclin E and CDK2 phosphorylated forms in Vero, HEp-2 and HEK 293 T cells in presence of DPIT. Fig. 4 A-D shows that, after treatment, the expression of the phosphorylated form of CDK2 was inhibited in both normal and tumor cells in the presence of DPIT, compared to the untreated cells, with the most remarkable effect in HEK 293 T transformed cells. Similarly, compared to the untreated cells, DPIT was able to inhibit the expression of the phosphorylated form of cyclin E in both normal and tumor cell lines considered. Any significant difference was observed between the two tumor cell lines, whereas the reduction of the hyperphosphorylation of pRB expression levels was more evident in Vero cells.

2.4. Specific inhibition of E2F pathway mediated by DPIT

Finally to further confirm the *in silico* molecular modeling studies and the biological data, we employed a model in which stimulated-E2F pathway can be affect by DPIT activity. E2F family members are transcription factors that play important roles in cell cycle regulation, since they are involved in the transition from G1 to S phase. The E2F proteins are heterodimers which are inactivated by binding to Retinoblastoma proteins (pRb), that act as transcriptional repressors. The hypophosphorylation of pRb, mediated by CDK2/cyclin E, has an antiproliferative activity by associating with transcription factors of the E2F members and thereby prevents transactivation of genes required for S phase entry such as CDK2/cyclin E complex itself. It is well known that the Epidermal Growth Factor (EGF) induces both cell growth and proliferative events, acting on the E2F transcription factor. In order to investigate if the antiproliferative activity of DPIT can act on E2F pathway, we employed a 293T cells as a model in which E2F pathway was specifically induced by using EGF, and the activity of the pathway was evaluated by a E2F-Cignal Reporter Assay System. HEK 293 T cells were co-transfected with both a primary and a control reporter for 16 hours, followed by an overnight incubation with EGF 100 ng/mL in presence or not of DPIT (10 μM or 100 μM). Cells treated with EGF were used as controls. Results showed in Fig. 5 clearly indicated that DPIT reduced E2F pathway activation, compared to the control, in a concentration dependent manner. This finding suggests that DPIT could control the E2F mediated transcriptional activity, affecting cell proliferation of tumor HEK 293 T cells.

Journal Name RSCPublishing

ARTICLE

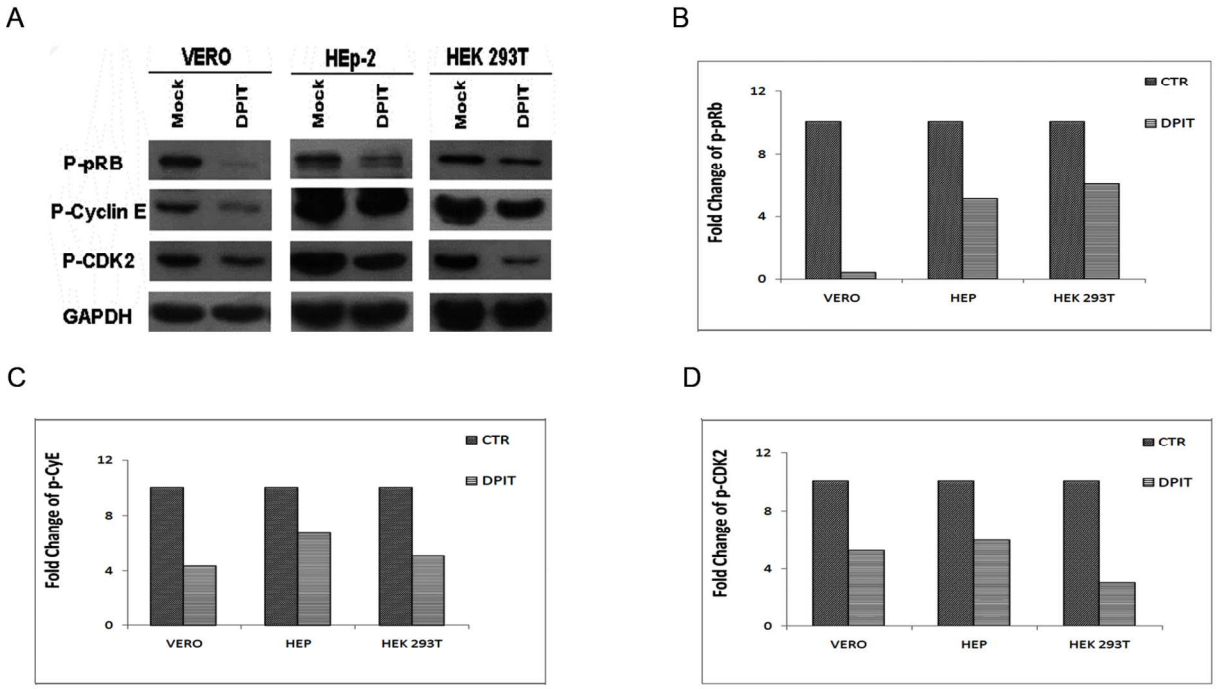

Fig. 4 VERO, HEp-2 and HEK 293 T cells were incubated with 100 μM of DPIT and collected 24 h. Total protein extractions were obtained as described in Materials and Methods. Equal amount of protein extracts were resolved in 10 % SDS polyacrilammide gel and transferred into nitrocellulose membrane. The membranes were probed with phospho-pRb, phospho-cyclin E, phospho-CDK2 and GAPDH antibodies (A). GAPDH was used as loading control. Graphic representation of fold changes of phosphorylated pRb, cyclin E and CDK2 was obtained by using T.I.N.A program (B-D).

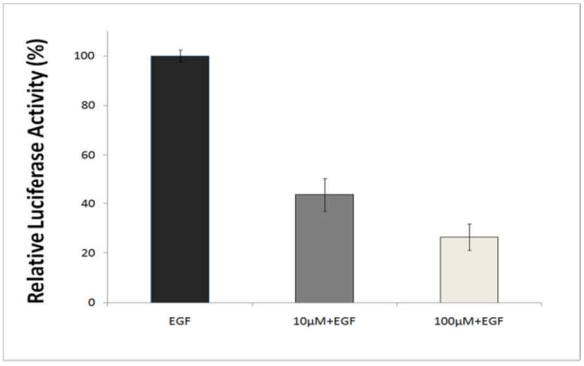

Fig. 5 Transfected HEK 293T cells are incubated with DPIT at concentration of 10 and 100 μM and cell growth was induced by using Epidermal Growth Factor (EGF). The cells were analyzed to evaluate the activity of reporter gene under the control of E2F basal promoter element by using Dual-Glo® Luciferase Assay, as described in Materials and Methods. [The y axis represents the relative Luciferase activity (%); the x axis represents the cells exposed to EGF (EGF); the cells exposed to EGF and treated with 10 μM of DPIT (10 μM+EGF), and the cells exposed to EGF and treated with 100 μM of DPIT (100 μM+EGF)]. Error bars indicate the means ± SD of three independent experiments.

3. Experimental

3.1. Preparation of Proteins and Ligands

The crystal structures of CDK2-ligand complex (PDB ID: 3F5X, 3EZV, 4ERW, 3PXF, 3PY1) were retrieved from the PDB_REDO databank as fully optimized ones.[24] The PDB_REDO procedure combine re-refinement and rebuilding within a unique decision-making framework to improve structures, using a variety of existing and custom built software modules to choose an optimal refinement protocol (e.g. anisotropic, isotropic or overall B-factor refinement, TLS model) and to optimize the geometry versus data-refinement weights. Next, it proceeds to rebuild side chains and peptide planes before a final optimization round.[25] From these refined structures were deleted all water molecules and unwanted ones (ions, glycol, etc.) and for 3F5X were retained only A and B chains. Only for docking procedure, the 3D structures of ligands were extracted from the PDB files whereas these of the eight stereoisomers of DPIT were built using Winmostar (4.101) software[26] and all geometries were fully optimized, in the same software, with the semi empirical PM7[27] Hamiltonian implemented in MOPAC2012 (14.04W).[28]

3.2. Molecular Dynamics Simulations

The molecular dynamics simulations of the CDK2/ligand complexes (based on the PDBs prepared as described above) were performed

with the YASARA Structure package (13.9.8).[29] A periodic simulation cell with boundaries extending 10 Å from the surface of the complex was employed. The box was filled with water, with a maximum sum of all bumps per water of 1.0 Å, and a density of 0.997 g/mL with explicit solvent. YASARA's pKa utility was used to assign pKa values at pH 7.2,[30] and the cell was neutralized with NaCl (0.9 % by mass); in these conditions EZV ligand results protonated at piperazinic *N*-Me. Waters were deleted to readjust the solvent density to 0.997 g/mL. The YAMBER3 force field was used with long-range electrostatic potentials calculated with the Particle Mesh Ewald (PME) method, with a cutoff of 7.86 Å.[31-33] The ligand force field parameters were generated with the AutoSMILESutility,[34] which employs semiempirical AM1 geometry optimization and assignment of charges, followed by assignment of the AM1BCC atom and bond types with refinement using the RESP charges, and finally the assignments of general AMBER force field atom types. Optimization of the hydrogen bond network of the various CDK2-ligand complexes was obtained using the method established by Hooft et al.,[35] in order to address ambiguities arising from multiple side chain conformations and protonation states that are not well resolved in the electron density.[36] A short MD was run on the solvent only. The entire system was then energy minimized using first a steepest descent minimization to remove conformational stress, followed by a simulated annealing minimization until convergence (<0.01 kcal/mol Å). The MD simulation was then initiated, using the NVT ensemble at 298 K, and integration time steps for intramolecular and intermolecular forces every 1.25 fs and 2.5 fs, respectively. The MD simulation was stopped after 1 ns and, on the last frame, a second cycle of energy minimization, identical to the first, was applied.

3.3. Docking Protocol

Macromolecules and ligands, as obtained after MD simulation and energy minimization, were prepared with Vega ZZ[37] (3.0.3.18) assigning Gasteiger charges to protein and AM1BCC ones to ligand. Docking was performed with AutoDock (4.2.5.1) software,[38] which has been used widely because it shows acceptable free energy values relative to experimentally observed docking data.[39] To define all binding sites and to have structural inputs, a grid based procedure was used.[40] Here the output was saved as a PDBQT. The grid box was set, and the output was saved as a .gpf file. The ligand-centered maps were generated by the program AutoGrid (4.2.5.1)with a spacing of 0.286 Å (0.375 Å for 3PY1) and dimensions that encompass all atoms extending 10 Å from the surface of the complex (for 3PY1 both types 1 and 3 catalytic sites were included in the box). All of the parameters were inserted at their default settings. In the docking tab, the macromolecule and ligand are selected, and GA parameters are set as ga_runs =100, ga_pop_size = 150,ga_num_evals = 25000000, ga_num_generations = 27000, ga_elitism = 1, ga_mutation_rate = 0.02, ga_crossover_rate = 0.8, ga_rossover_mode = two points, ga_cauchy_alpha = 0.0, ga_cauchy_beta = 1.0, number of generations for picking worst individual = 10, output is selected as LamarckianGA, and the file is saved as .dpf.

3.4. Cell lines

VERO cells (American Type Culture Collection) were propagated in Dulbecco's modified Eagle's medium (DMEM; Gibco/Invitrogen Corporation, Grand Island, NY) supplement with 6 % fetal bovine serum (FBS; Lonza, Belgium) and mixture 100 U/mL penicillin and 100 mg/mL streptomycin. HEp-2 cells (human larynx epidermoid carcinoma cell line) and HEK 293T (Human Embryonic Kidney) were grown in Dulbecco's modified Eagle's medium (DMEM; Gibco/Invitrogen Corporation, Grand Island, NY) supplemented with 10 % of fetal bovine serum, 100 U/mL penicillin and 100 mg/mL streptomycin. All cells line were incubated at 37 ° C under 5 % CO_2.

3.5. Antibody

Polyclonal antibodies against glyceraldehyde-3-phosphate dehydrogenase (GAPDH), phosphorylated forms of cyclin E (Thr395), phosphorylated forms of CDK2 (Thr14/Tyr15) and phosphorylated form of pRb were purchased from Santa Cruz Biotechnology. Secondary antibodies anti-rabbit and anti-mouse IgG peroxidase-conjugated were purchased from Santa Cruz Biotechnology (Santa Cruz, CA).

3.6. Cell viability assay

CellTiter-Glo® Luminescent Cell Viability Assay Kit (Promega) was used to evaluate cell viability in all cell lines tested. 10000 cells were plates in 96-well plates in Dulbecco's modified Eagle's medium supplement with 6 % FBS and incubate at +37°C. After 24h the cells were treated or mock treated with 80, 90, 100 µM of DPIT and collected at 24 h, 48 h and 72 h. The proliferation assay was performed according to the protocol CellTiter-Glo® Luminescent Cell Viability Assay Kit (Promega). Briefly equal volume of Cell Titer-Glo Reagent was added to the cells and mixed for 2 minutes on orbital shaker. After stabilization at room temperature for 10 minutes, the luminescent signal, were determinate by GLOMAX 96 Microplate Luminometer (Promega). The values obtained were used to calculated the percentage of cell viability as follow: [(cells untreated value)-(cells treated value)/(cells untreated value)]x 100.

3.7. Western Blot analysis

VERO, HEp-2 and HEK 293T cell lines were treated for 24 h with DPIT at final concentration of 100 µM. After 24 h all samples were collected and centrifuged at 1500 rpm for 5 minutes. The pellets were washed with 1 mL of PBS 1x washed and lysed using SDS Sample Buffer 1x (62,5 mM Tris-HCl pH 6.8; DTT 1M; 10 % Glycerol; 2 % di SDS; 0,01% bromophenol blue). Equal amount of proteins extract was resolved in 10 % SDS polyacrylamide gel and then transferred into nitrocellulose membrane (Bio-Rad). The membrane was washed with TBS + Tween 0,01 % (TTBS: 20mM Tris-HCl pH 8.0; 0.9 % NaCl; 0.1 % Tween 20) and 5 % of not fat dry milk and incubated over night at +4°C with specific primary antibody diluted 1:1000. After overnight incubation the membrane was incubated with anti-rabbit IgG or anti-mouse IgG peroxidase conjugate and the reaction was revealed by using the kit SuperSignal West Pico as a chemiluminescent substrate (Thermo Scientific, Rockford, IL).

3.8. Evaluation of E2F pathway activity after stimulation with the epidermal grown factor (EGF)

The Cignal Reporter Assay coupled with Dual-Glo® Luciferase Assay System were used to evaluate the E2F pathway activity after induction with epidermal grown factor (EGF). HEK 293T cells were inoculated in 96 well plate and transfected with Reverse Transfection Method. Reverse Transfection was applied using Fugene HD (Promega) as transfected agent in 50 µL Opti-MEM® (Gibco/Invitrogen Corporation, Grand Island, NY) and 50 µL of the diluted nucleic acids (1:1 ratio), mixed gently and incubate 20 minutes at room temperature (RT). After incubation 50 µL of HEK 293T suspension cells contained 8 x 10^4 cells in Opti-MEM mixed contained 10% of FBS. After 16 h of reverse transfection the medium was changed with complete growth medium and cells were incubate with DPIT at concentration of 10 and 100 µM for 24 hours in presence of EGF (100 ng/mL) as strong inducer of E2F pathway. Untreated cells incubated with EGF were used as positive control

(EGF-cells). After incubation luciferase activity was measured using the Dual Luciferase Assay system (Promega) on a Glomax multi luminometer (Promega). The renilla/firefly luciferase ratio was calculated from the mean luminescence values of triplicate wells, after blanking against values from untransfected cells and the fold changes were calculated as follow: [(EGF-cells untreated value)-(EGF-cells treated value)/(EGF-cells untreated value)]x 100.

4. Conclusions

The aims of this study were to examine the effect of DPIT on cellular proliferation and the possible mechanisms involved in this regulation. To address this issue a docking analysis was performed to characterize its capability to inhibit CDK2, as well as to explore the details of their dominant interactions. Thus the DPIT was taken as the template molecule in this process, and the results are shown in Fig. 3. In addition to verify the *in silico* data, we designed experiments using tumor cells such as HEp-2 and HEK 293T cells and non-tumor Vero cells. Our results showed that DPIT treatment significantly decreased the cell growth in a dose-dependent manner in both tumor and non-tumor cells. In particular the presence of DPIT seems to interfere with the normal progression from G1 to S phase by negatively regulating the cyclin dependent kinases 2 and its substrate, cyclin E.

Consistent with this data the marked growth inhibitory effects observed in these cells likely indicated an addiction to CDK2. To address the possible roles of DPIT in cellular proliferation by regulating the progression from G1 to S phase, we used EGF factor to specifically induce E2F which have a clearly defined role as key transcription factor necessary for cell growth, DNA repair and differentiation. EGF treatment on HEK 293T cells in the presence of DPIT demonstrated that it is able to reduce the activity of the transcription factor E2F in a dose dependent manner (Fig. 5).

In conclusion, the obtained results reveal that DPIT can interact with CDK2 occupying the allosteric site and, to the best of our knowledge, it would be the first instance in which one single molecule is capable of this, because the inhibitor ANS acts as a couple. Unfortunately its low activity does not allow an immediate use, but could be considered as a parent for obtaining compounds much more efficient by making appropriate changes. However decorated 6,6',7,7'-tetrahydro-1*H*,1'*H*-2,3'-biindoles, such as DPIT, by targeting CDK2 seem to be an attractive scaffold for development of useful anticancer drugs, establishing the broad pharmacologic impact of targeting the CDK2/cyclin E complex in cancer cells.

Acknowledgements

This work was partially supported by MIUR (project PRIN 20109Z2XRJ_010).

Notes and references

[a] *Dipartimento di Scienze del Farmaco, Università di Catania, V.le A. Doria, 95125 Catania, Italy.*

[b] *Dipartimento di Scienze Chimiche, Università di Messina, V.le F. Stagno d'Alcontres 31, 98166 Messina, Italy. E-mail: ascala@unime.it; Tel/Fax: +39 090 393897.*

[c] *Dipartimento di Scienze Biologiche ed Ambientali, Università di Messina, V.le F. Stagno d'Alcontres 31, 98166 Messina, Italy. E-mail: mtsciortino@unime.it; Tel: +39 090 6765217.*

[d] *CNR-ISMN Istituto per lo Studio dei Materiali Nanostrutturati c/o Dipartimento di Scienze Chimiche dell'Università di Messina, V.le F. Stagno d'Alcontres 31, 98166 Messina, Italy.*

1. V. Kolupaeva and C. Basilico, *Cell Cycle,* 2012, **11**, 2557-2566.
2. B. Sebastian, A. Kakizuka and T. Hunter, *Proc. Natl. Acad. Sci. U. S. A.,*1993, **15**, 3521-3524.
3. Y. Li, W. Gao, F. Li, J. Wang, J. Zhang, Y. Yang, S. Zhanga and L. Yang, *Mol. BioSyst.,* 2013, **9**, 2266-2281.
4. G. I. Shapiro, *J. Clin. Oncol.,* 2006, **24**, 1770-1783.
5. C. McInnes, *Drug Discovery Today Abstract,* 2008, **13,** 875-881.
6. E. Altieri, M. Cordaro, G. Grassi, F. Risitano and A. Scala, *Tetrahedron*, 2010, **66,** 9493-9496.
7. E. Altieri, M. Cordaro, G. Grassi, F. Risitano and A. Scala, *Synlett.,* 2010, **14,** 2106-2108.
8. M. Cordaro, G. Grassi, F. Risitano and A. Scala, *Synlett.,* 2009, **1**, 103-105.
9. M. Cordaro, G. Grassi, F. Risitano and A. Scala, *Tetrahedron,* 2010, **66**, 2713-2717.
10. M. Cordaro, G. Grassi, A. Rescifina, U. Chiacchio, F. Risitano and A. Scala, *Tetrahedron,* 2011, **67**, 608-611.
11. M. Cordaro, F. Risitano, A. Scala, A. Rescifina, U. Chiacchio and G. Grassi, *J. Org. Chem.,* 2013, **78**, 3972-3979.
12. A. Scala, M. Cordaro, F. Risitano, I. Colao, A. Venuti, M. T. Sciortino, P. Primerano and G. Grassi, *Mol. Divers.*, 2012, **16**, 325-333.
13. A. Scala, M. Cordaro, G. Grassi, A. Piperno, G. Barberi, A. Cascio, and F. Risitano, *Bioorg. Med. Chem.,* 2014, **22**, 1063-1069.
14. A. Scala, M. Cordaro, A. Mazzaglia, F. Risitano, A. Venuti, M. T. Sciortino and G. Grassi, *Mol. Divers.,* 2013, **17**, 479-488.
15. A. Scala, M. Cordaro, A. Mazzaglia, F. Risitano, A. Venuti, M. T. Sciortino and G. Grassi, *Med. Chem. Commun.,* 2011, **2**, 172-175.
16. F. Pin, F. Buron, F. Saab, L. Colliandre, S. Bourg, F. Schoentgen, R. Le Guevel, C. Guillouzo and S. Routier, *Med. Chem. Commun.,* 2011, **2,** 899-903.
17. G. Cozza, A. Bortolato, E. Menta, E. Cavalletti, S. Spinelli and S. Moro, *Anticancer Agents Med. Chem.,* 2009**, 9**(7), 778-786.
18. J. M.; Zhang, P. L. Yang and N. S. Gray, *Nat. Rev. Cancer,* 2009**, 9**(1), 28-39.
19. J. I. Trujillo, J. R. Kiefer, W. Huang, A. Thorarensen, L. Xing, N. L. Caspers, J. E. Day, K. J. Mathis, K. K. Kretzmer, B. A. Reitz, R. A. Weinberg, R. A. Stegeman, A. Wrightstone, L. Christine, R. Compton and X. Li, *Bioorg. Med. Chem. Lett.,* 2009, **19**(3), 908-911.
20. S. Betzi, R. Alam, M. Martin, D. J. Lubbers, H. J. Han, S. R. Jakkaraj, G. I. Georg and E. Schonbrunn, *ACS Chem. Biol.,* 2011**, 6**(5), 492-501.
21. N. R. Brown, M. E. M. Noble, A. M. Lawrie, M. C. Morris, P. Tunnah, G. Divita, L. N. Johnson and J. A. Endicott, *J. Biol. Chem.,* 1999, **274**(13), 8746-8756.
22. R. Honda, E. D. Lowe, E. Dubinina, V. Skamnaki, A. Cook, N. R. Brown and L. N. Johnson, *EMBO J.,* 2005**, 24**(3), 452-463.
23. P. D. Jeffrey, A. A. Ruso, K. Polyak, E. Gibbs, J. Hurwitz, J. Massague, N. P. Pavletich, *Nature ,* 1995**, 376**(6538), 313-320.
24. http://www.cmbi.ru.nl/pdb_redo/.
25. R. P. Joosten, K. Joosten, G. N. Murshudov and A. Perrakis, *Acta Crystallographica Section D-Biological Crystallography,* 2012**, 68,** 484-896.
26. N. Senda, *Idemitsugihou,* 2006**, *49*(1)**, 106.
27. J. J. P. Stewart, *Journal of Molecular Modeling.,* 2013**, 19**(1), 1-32.
28. J. J. P. Stewart, MOPAC2012. HTTP://OpenMOPAC.net.

29. E. Krieger, *YASARA*, 13.9.8; YASARA Biosciences GmbH: Vienna, Austria, 2013.
30. E. Krieger, J. E. Nielsen, C. A. Spronk and G. Vriend, *J. Mol. Graphics Modell.,* 2006, **25**(4), 481-486.
31. W. D. Cornell, P. Cieplak, C. I. Bayly, I. R. Gould, K. M. Merz, D. M. Ferguson, D. C. Spellmeyer, T. Fox, J. W. Caldwell, and P. A. Kollman, *J. Am. Chem. Soc.,* 1995**, 117**(19), 5179-5197.
32. U. Essmann, L. Perera, M. L. Berkowitz, T. Darden, H. Lee and L. G. Pedersen, *J. Chem. Phys.,* 1995**, 103**(19), 8577-8593.
33. Y. Duan, C. Wu, S. Chowdhury, M. C. Lee, G. M. Xiong, W. Zhang, R. Yang, P. Cieplak, R. Luo, T. Lee, J. Caldwell, J. M. Wang and P. Kollman, *J. Comput. Chem.,* 2003**, 24**(16), 1999-2012.
34. A. Jakalian, D. B. Jack and C. I. Bayly, *J. Comput. Chem.,* 2002**, 23**(16), 1623-1641.
35. E. Krieger, R. Dunbrack, R. Hooft and B. Krieger, *Computational Drug Discovery and Design,* 2012**, 819,** 405-421.
36. R. W. W. Hooft, G. Vriend, C. Sander and E. E. Abola, *Nature,* 1996**, 381**(6580), 272.
37. A. Pedretti, L. Villa and G. Vistoli, *J. Comput. Aided Mol. Des.,* 2004**, 18**(3), 167-173.
38. G. M. Morris, R. Huey, W. Lindstrom, M. F. Sanner, R. K. Belew, D. S. Goodsell and A. J. Olson, *J. Comput. Chem.,* 2009**, 30**(16), 2785-2791.
39. B. Gorelik and A. Goldblum, *Proteins-Structure Function and Bioinformatic,* 2008, **71**(3), 1373-1386.
40. P. J. Goodford, *J. Med. Chem.* 1985**, 28**(7), 849-857.
41. A. C. Wallace, R. A. Laskowski and J. M. Thornton, *Protein Eng.* 1995**, 8**(2), 127-134.

Decorated 6,6',7,7'-tetrahydro-1*H*,1'*H*-2,3'-biindoles, such as DPIT, by targeting CDK2 seem to be an attractive scaffold for development of useful anticancer drugs.